How Well Does the Hole Burning Action Spectrum Represent the Site-Distribution Function of the Lowest-Energy State in Photosynthetic Pigment-Protein Complexes?

Valter Zazubovich[1,*], Ryszard Jankowiak[2]

[1]Department of Physics, Concordia University, 7141 Sherbrooke Str. West, Montreal H4B 1R6, Quebec, Canada; [2]Department of Chemistry, Kansas State University, Manhattan KS, 66506 USA.

*Corresponding author: valter.zazubovits@concordia.ca

Abstract: For the first time, we combined Monte-Carlo and nonphotochemical hole burning (NPHB) master equation approaches to allow for ultra-high resolution (<0.005 cm^{-1}, smaller than the typical homogeneous line widths at 5 K) simulations of the NPHB spectra of dimers and trimers of interacting pigments. These simulations reveal significant differences between the zero-phonon hole (ZPH) action spectrum and the site-distribution function (SDF) of the lowest-energy state. The NPHB of the lowest-energy pigment, following the excitation energy transfer (EET) from the higher-energy pigments which are excited directly, results in the shifts of all excited states. These shifts affect the ZPH action spectra and EET times derived from the widths of the spectral holes burned in the donor-dominated regions. The effect is present for a broad variety of realistic anti-hole functions and it is maximal at relatively low values of inter-pigment coupling ($V \leq 5$ cm^{-1}) where the use of the Förster approximation is justified. These findings need to be considered in interpreting various optical spectra of photosynthetic pigment-protein complexes for which SDFs (describing the inhomogeneous broadening) are often obtained

directly from the ZPH action spectra. Water-soluble chlorophyll-binding protein (WSCP) was considered as an example.

1. Introduction:

Site selective spectroscopy techniques, including spectral hole burning (SHB) [1,2], fluorescence line narrowing (FLN) [3,4], and a combination of SHB and FLN (Δ-FLN[5-8]), provide important information about the properties of photosynthetic pigment-protein complexes at low temperatures[9]. This includes excited state lifetimes and their distributions, the shapes of the phonon sidebands (PSB; used in excitation energy transfer (EET) calculations as they affect spectral overlaps), the magnitude of the electron-phonon and electron- localized vibration couplings, site distribution function (SDF; which describes the probability of finding a pigment with a particular zero-phonon transition energy), protein energy landscape parameters, etc. Specifically, the EET rates are proportional to the spectral hole (line) widths, while the zero-phonon hole (ZPH) action spectrum is generally believed to represent the SDF of the lowest-energy state. Recently, we extended the non-photochemical hole burning (NPHB) model described in detail in [10-12] and included the wavelength-dependent distributions of the EET rates and the NPHB of the lower-energy (lower-E) pigments following the EET from the directly-excited higher-energy pigments or states[13,14]. An important feature of NPHB is that upon illumination the absorption of the molecules in resonance with the excitation is not destroyed, but instead shifted to other wavelengths due to some conformational changes in the pigment's local environment. The applicability of this model [13,14] has been successfully tested for the lowest-E band of the Fenna-Matthew-Olson (FMO) complex, which is mostly contributed to by three identical lowest-E bacteriochlorophyll (Bchl *a*) pigments of the individual monomers of the

FMO trimer[15], as well as for dimeric Cytochrome b_6f [16]. These systems exhibit inter-pigment couplings on the order of several cm^{-1} or even less than 1 cm^{-1}, respectively. Modeling of the broad non-resonant NPHB features in the more strongly coupled systems using the distribution functions was reported in [17,18]. Both non-resonant and resonant NPHB were modeled using Monte-Carlo style excitonic calculations in [19,20] with spectral resolution of about 1 cm^{-1}, potentially overlooking some details that could manifest in the experiments performed at better spectral resolution. In this paper we combine approaches based on Monte-Carlo simulations and the NPHB master equation [9,10], achieving spectral resolution of < 0.005 cm^{-1}, several times smaller than the homogeneous dephasing-limited line widths typically observed at 5 K in EET-free cases. The goal is to properly account for the shifts of the higher-energy (higher-E) excited states following the NPHB of the lower-E pigments. This effect is well-known and has been explored in the case on non-resonant NPHB, but we present the first simulations with resolution high enough to model the influence of this effect on the ***resonant*** NPHB. As we will show, the largest effect on resonant holes and ZPH action spectra was observed for the inter-pigment couplings $V \leq 5$ cm^{-1}. According to [21,22], this value is well within the limits of applicability of the Förster theory [23] (except for a small fraction of complexes where pigments have identical transition energies). In this regime excitations are still mostly localized on single pigments but changes in the diagonal elements of the excitonic Hamiltonian do affect its eigenenergies to a noticeable degree. In other words, shifts of the higher-E excited states upon NPHB of the lower-E pigments exceed the EET-limited line (hole) widths and, thus, present an additional contribution to the resonant NPHB, for which we use the term “indirect burn” throughout this manuscript. We will discuss how this indirect burn influences the interpretation of the

experimental results, especially in terms of excited state lifetimes and SDF shapes, using Water-Soluble Chlorophyll-Binding Protein (WSCP) [24,25] as an example.

2. Model and Software.

The software employed here is a further development of the one used in [13,14]. (The reader interested in the technical details is referred to the Supplementary section.) The calculations of the spectral holes were based on the NPHB master equation[9] (Eq.S2) with EET-dependent NPHB yield

$$\phi(\lambda, \tau_{EET}) = \frac{\Omega_0 \exp(-2\lambda)}{\Omega_0 \exp(-2\lambda) + \tau_{fl}^{-1} + \tau_{EET}^{-1}}, \quad (1)$$

where τ_{fl} is the EET-free fluorescence lifetime (set to 2.5 ns) and τ_{EET} is the EET time. The tunneling parameter λ is generally subject to distribution [9], but in order to reduce calculation time the average NPHB rate of $\Omega_0\exp(-2\lambda)\approx 35000\ s^{-1}$ was employed instead. Although in most cases we did not utilize the λ-distributions in the calculations reported in this manuscript, our computational resources were sufficient for calculating the spectra in the presence of both the EET rate distribution and a single-tier λ-distribution. We verified that introduction of a λ-distribution with realistic parameters does not diminish the importance of the indirect burn effect, under reasonable assumptions that λ-distribution is independent on wavelength and is not correlated with the EET rate distribution. To the best of our knowledge it has never been explored if λ-distribution depends on wavelength within the inhomogeneously broadened band of the pigments that are located in the same protein pocket. The λ-distribution does not change much with wavelength in glassy hyperquenched water, ethanol and ortho-dichlorobenzene [11,26].

Examples of the calculations including the λ-distribution are reported in the Supplemental section (Figure S2).

Unlike in [13,14], the sub-SDFs of pigment/state subsets featuring EET rates within certain ranges (including the zero-rate sub-SDF for the energy acceptors) were calculated using a Monte-Carlo procedure. The site energies (the diagonal elements of the Hamiltonian) for over $5 \cdot 10^8$ dimers or trimers were randomly selected from the SDF of the respective pigments. The eigenvalues of the respective Hamiltonians were determined, yielding the lists of energies of the excited states. These states were, in most cases, localized due to site energy disorder. The fraction of the aggregates with nearly identical diagonal energies was small. The sets of eigenenergies were used to determine the EET rates for each complex from the spectral overlaps and to create, via binning and interpolation, the high-resolution (as good as 0.0048 cm^{-1}) sub-SDF (each for a particular range of the EET rates) employed in the subsequent modeling of the NPHB spectra. Förster theory [27,28] was used to calculate the EET rates and homogeneous zero phonon line (ZPL) widths, yielding EET contributions to ZPL widths $\Gamma_{EET} \sim V^2$ (Eq.S1). The parameters of the single-site spectra were previously employed to fit the Δ-FLN spectra of Cyt b_6f [29] and/or WSCP [24].

In a system of interacting pigments, the higher-E pigment may experience NPHB (with the probability reduced according to Eq.1) and/or transfer energy to the lower-E pigment; the latter may experience NPHB. The NPHB of the lowest-E pigment results in the shifts of all the excited states of the system. The software maintained the lists of the zero-phonon transition energies of the pigments and of the energies of the excited states before and after the NPHB of the lowest-E pigment. The doublets or triplets of the eigenenergies were sorted and the pigment dominating the lowest-E state was selected. This pigment was assumed to experience NPHB

when the lowest-E state was burned. To simulate the NPHB, the site energy of this pigment was changed by adding a shift randomly selected from a distribution representing the anti-hole function describing how the absorption of the molecules with ZPL initially at the same wavelength is redistributed by NPHB. In the case of a dimer there are three possible scenarios involving NPHB of the lower-E pigment (Figure 1): *(i)* The lower-E pigment may shift to the red. This will result in a small red shift of the higher excited state, not exceeding *V*. The lower-E pigment remains lower-E one; *(ii)* The lower-E pigment of a dimer may shift to the blue, but still remain the lower-E pigment; this will result in the blue shift of the higher excited state by up to one *V*; *(iii)* the lower-E pigment may shift enough to the blue to become the higher-E pigment. If this occurs, the state preferentially localized on the initially higher-E pigment will shift to the red by up to 2*V*, and will become the lower-E state.

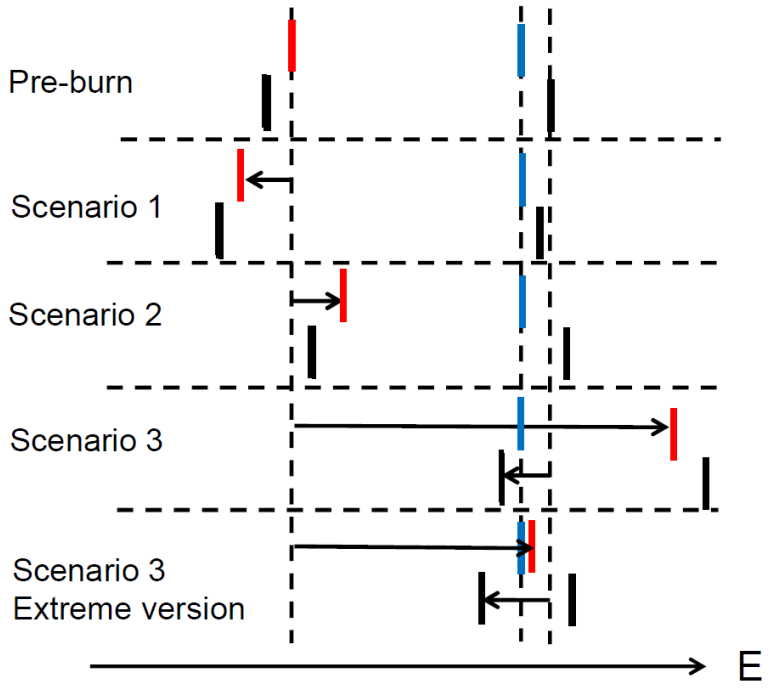

Figure 1. Various scenarios for the shifts of the (localized) excited states (black bars) in a dimer, depending on the NPHB-induced spectral shift of the lower-energy pigment (red bar). The site energy of the pigment that before NPHB was the higher-energy pigment is represented by a blue bar.

The excited states were then recalculated and the distributions of the higher-state shifts resulting from the lower-state NPHB were determined for multiple energies within the range limited by the SDF. The distributions of the higher-E state shifts were calculated separately for every (range of) EET rate using binning, and for multiple values of burn frequency ω_B. The shift distributions for other burn frequencies were obtained from the binned ones by linear interpolation. The burning into the higher-energy state(s) was modeled as a two-step process. First, "direct" NPHB with the yield affected by EET (Eq. 1) and the original broad and smooth anti-hole function was employed. Second, the indirect NPHB step with the anti-hole function(s), such as those shown in Figure 2, was added. The rate of this process ("indirect burn") was assumed to be nearly equal to the lowest-state NPHB rate; it was corrected only for possible energy losses due to the direct emission from the higher-E states. These losses are significant only for $V < 5$ cm^{-1} [13,14].

Summarizing, the software employed here represents a new hybrid approach to modeling the site-selective optical spectra that includes both Monte-Carlo simulations and NPHB master equation features. Calculations were performed on a personal computer with an Intel Core i7 7th generation processor and 32GB of RAM. The software was written in MS Visual Basic and has been continuously improved and expanded since 2006 (available upon request).

3. Results

3.1. Higher-Energy State Shift Distributions.

The examples of the distributions of the higher-E state shifts are shown in Figure 2, where frames A and B present the shift distributions for two different NPHB anti-hole functions;

otherwise, the parameters were identical, corresponding to a homodimer with Γ_{inh}=250 cm^{-1} and S_{ph}=0.72. Γ_{inh} is the width of the SDF, i.e. the extent of the inhomogeneous broadening determined by the static transition energy disorder. S_{ph} is the Huang-Rhys factor for protein phonons, the electron-phonon coupling strength. It is the average number of phonons excited in an electronic transition. To improve the signal to noise ratio, each curve in Figure 2 was obtained by adding together the curves for all EET rates at one particular ω_B. The respective shift distributions for other values of V generally were similar to those presented here, but with the range of shifts being stretched or contracted. In the case of a homo-trimer the shape and burn frequency dependence of the shift distributions for both the middle- and the highest-E states were also fairly similar (data not shown). When the anti-hole function is the full SDF for low enough ω_B the most likely scenario involves higher-E pigment becoming the lower-energy one (scenario 3 from Figure 1; see thick magenta curve in Figure 2A). As ω_B is increasing, scenario 3 becomes less and less likely, and the higher-state shift distribution ends up peaked around ω_B (scenarios 1 and 2; see thick blue curve in Figure 2A as an example). When red spectral shifts upon NPHB are very unlikely (Frame B), for low ω_B scenario 3 (pigments switching order) will be dominant, while for high ω_B scenario 2 (small blue shifts) will be dominant. Scenario 1 (small red shift) is extremely unlikely in the latter model. Arrows in Figure 2 indicate the direction in which various features of higher-state shift distributions increase with the increase or decrease of ω_B.

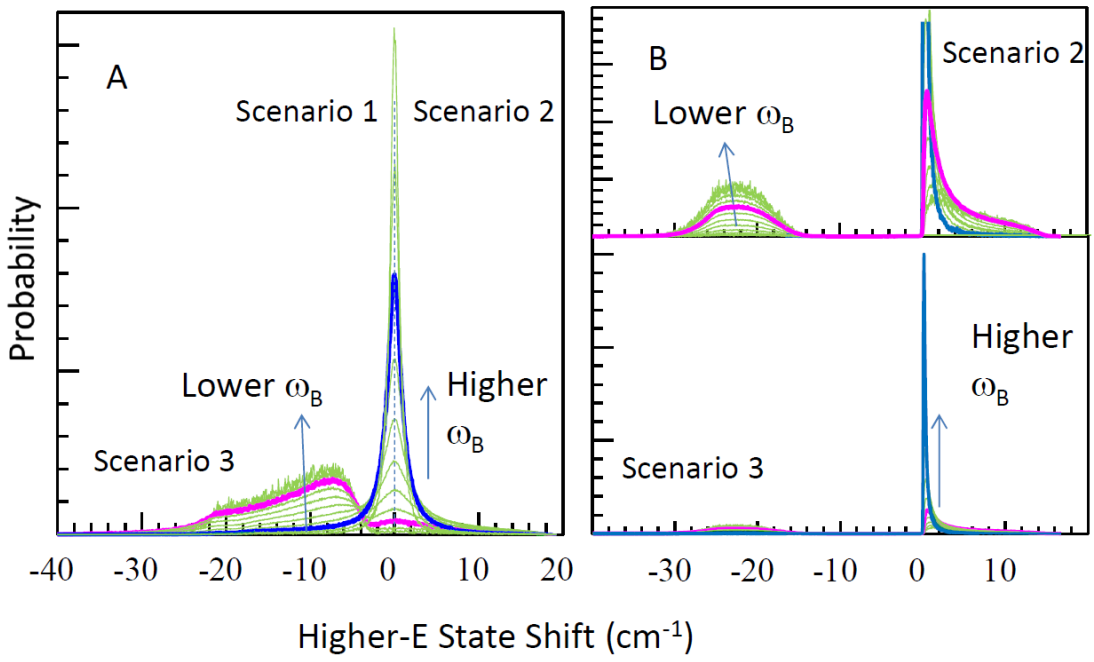

Figure 2. Frame A: Distributions of the shifts of the higher-E state of a homodimer (SDF width 250 cm^{-1}) for the case where the lowest-E pigment's NPHB anti-hole function is equal to the full SDF; V=20 cm^{-1}. The curves were normalized to the same area. "Scenarios" refer to Figure 1 and respective text. **Frame B:** The same parameters as in Frame A, but with the anti-hole function for the "direct" NPHB being a Gaussian blue-shifted by 55 cm^{-1} and with a width of 40 cm^{-1}. The lower part of frame B shows the full vertical range of the shift distribution curves.

3.2. NPHB Spectra – SDF as the Anti-hole Function

Figure 3 presents calculated NPHB action spectra (dependence of the resonant hole on ω_B for fixed illumination dose) and examples of spectral holes obtained for a homodimer with WSCP parameters, anti-hole equal to the full SDF, and several values of V. The red and gray hole spectra in Frame A were calculated in both the absence and presence of the higher-state shifts (indirect burn), respectively. The red holes also include the "direct" NPHB contributions from the higher-E states (reduced according to Eq.1), and therefore all observed differences should be attributed to the indirect burn effect.

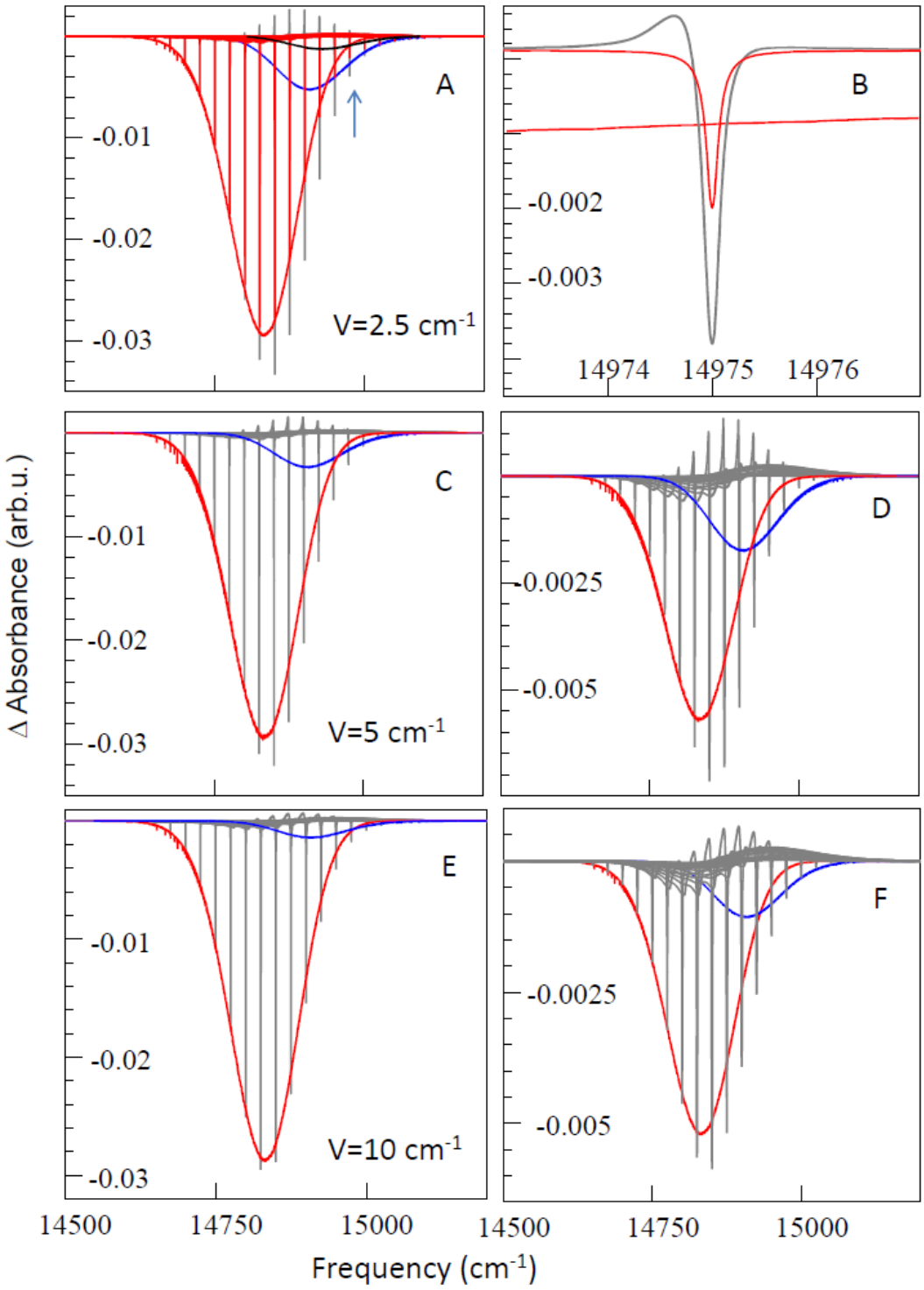

Figure 3. The anti-hole function is equal to the full SDF and WSCP parameters[24,30] were adopted in our calculations**.** The SDF was peaked at14870 cm^{-1} (672.5 nm) and had width of 165 cm^{-1}. The phonon sideband consisted of three lognormal contributions [30] with a combined S=0.81. Comparison of the ZPH action spectra in the presence (gray) and absence (red) of the "indirect burn" for *V*=2.5 cm^{-1} (Frame A). "Direct" burn into the acceptors and donors is included for both

red and gray holes. The arrow indicates the hole at 14975 cm^{-1}, shown in detail in Frame B. Frames C and E present the calculated ZPH action spectra for V=5 and 10 cm^{-1}, respectively, at the maximal resolution of our calculations (<0.005 cm^{-1}). Frames D and F show ZPH action spectra for V=5 and 10 cm^{-1}, but calculated assuming detection with the resolution of 1 cm^{-1}. Red solid broad curves are the sub-SDF of the acceptors. Black curve in Frame A represents the contribution from the direct burning into donor states. Blue curves represent the additional contribution to the ZPH action spectra due to indirect burn of the donor states. The fractional depths of the holes on the red side of the spectrum were about 35%.

For V=2.5 cm^{-1}, direct NPHB into the donors absorption was non-negligible, and the red hole spectra protruded deeper than the broad red curve (acceptor sub-SDF, see Frame B). Black curve in Frame A represents the contribution of the donor states to the direct burn. For V=1 cm^{-1} (not shown) direct NPHB into the donors absorption was the main contribution to the burning also at higher frequencies and the additional contribution of the indirect burn was small. For V=5 cm^{-1} and higher, the depths of the holes in the absence of the "indirect burn" closely followed the acceptor SDF. The differences in the ZPH action spectra were present but slightly less pronounced for the anti-hole model employed in Figure 2B - a Gaussian blue-shifted by 55 cm^{-1} and with the width of 40 cm^{-1}. The shifts of the higher excited states result in an increase of the resonant hole depths beyond what follows from Eq. 1 (red holes in Figure 3A). This should be remembered when utilizing the NPHB action spectra for the determination of the shapes of the SDF of the lowest-E states in the systems of interacting pigments. Specifically, in Figures 3A and C the peak of the calculated ZPH action spectrum (gray holes) differed from the peak of the acceptor SDF (broad red curve) by about 12 cm^{-1}, and further tailing was present at higher frequencies. 12 cm^{-1} is comparable to the product of the peak phonon frequency and electron-phonon coupling S, i.e. to the expected shift between the ZPH action spectrum and the emission spectrum. The difference between the ZPH action spectra and the acceptor SDF was clearly enhanced when the hole spectra were measured with a spectrometer whose bandwidth (1 cm^{-1})

was much larger than both the dephasing-limited line width and the bandwidth of the laser (Frames D and F), since the narrower holes burnt into the acceptor sub-SDF (red) were smoothed out more than the broader holes with significant indirect burn contribution. The difference between the depths of the red and gray spectral holes decreased again as the inter-pigment coupling increased to 10 and then to 20 cm^{-1} (not shown). This is in agreement with [19] where no difference was noticeable for $V = 50$ cm^{-1}. The Δ-FLN spectra, also calculated in the presence and absence of the indirect burn effect, differ mostly by magnitude, not by shape. Examples can be found in the Supplementary section.

3.3. WSCP as an Example.

Effects described here may explain some recent observations for Water-Soluble Chlorophyll-Binding Protein (WSCP) [24,25], where two strongly-coupled Chl dimers (that may contain either Chl *a* or Chl *b*) are weakly coupled to each other. While the emission spectrum appeared to originate from the terminal energy acceptors only (the lowest-energy state of the tetramer), the ZPH action spectrum had comparable contributions from the lowest-E states of both strongly-coupled dimers. Similar results were reported in [25,31] but it was unclear how many Chls were present in each reconstituted WSCP protein. A system like WSCP has to be treated in extended Förster approximation. Although the maximal coupling between the chlorophylls belonging to two different strongly-coupled dimers is estimated as 15-20 cm^{-1}, it is likely that due to interactions within these dimers the lowest-E states of each dimer have reduced transition dipoles (the oscillator strength of the lower band of WSCP is about 40% of that of the higher band and, therefore, one is likely dealing with weaker transition dipoles when one considers couplings between the lowest-E states of the two strongly-coupled dimers, effectively reducing V as $V \sim \mu^2$).

A decrease of the effective coupling is in agreement with the observed EET times of several picoseconds[25, 31]. Still, according to Eq.1, EET on a timescale of several ps should reduce the "direct" NPHB yield by about three orders of magnitude. One could also note that the hole spectra in [24] were clearly non-conservative. This was attributed to a quasi-photochemical hole-burning mechanism where an electron was temporarily transferred from a Chl *a* to a nearby aromatic residue such as tryptophane. If this were indeed the case, indirect burn effect in WSCP would feature an extreme version of Scenario 1 from Figure 1 (as the site energy of the lower-E pigment would be moved to about 830 nm with the formation of Chl^{+}). Figure 4 shows ZPH action spectra calculated for WSCP at two different resolutions (0.005 cm^{-1} and 1 cm^{-1}) for V=5 and 10 cm^{-1} assuming this burning mechanism. The action spectra closely resemble those in Frames C-F of Figure 3, except the anti-holes look different, as expected. Note that the NPHB action spectra were obtained with the resolution of 0.5 or 1.0 cm^{-1} in [24] and thus they should be compared to the data in Frames B and D rather than A and C of Figure 4.

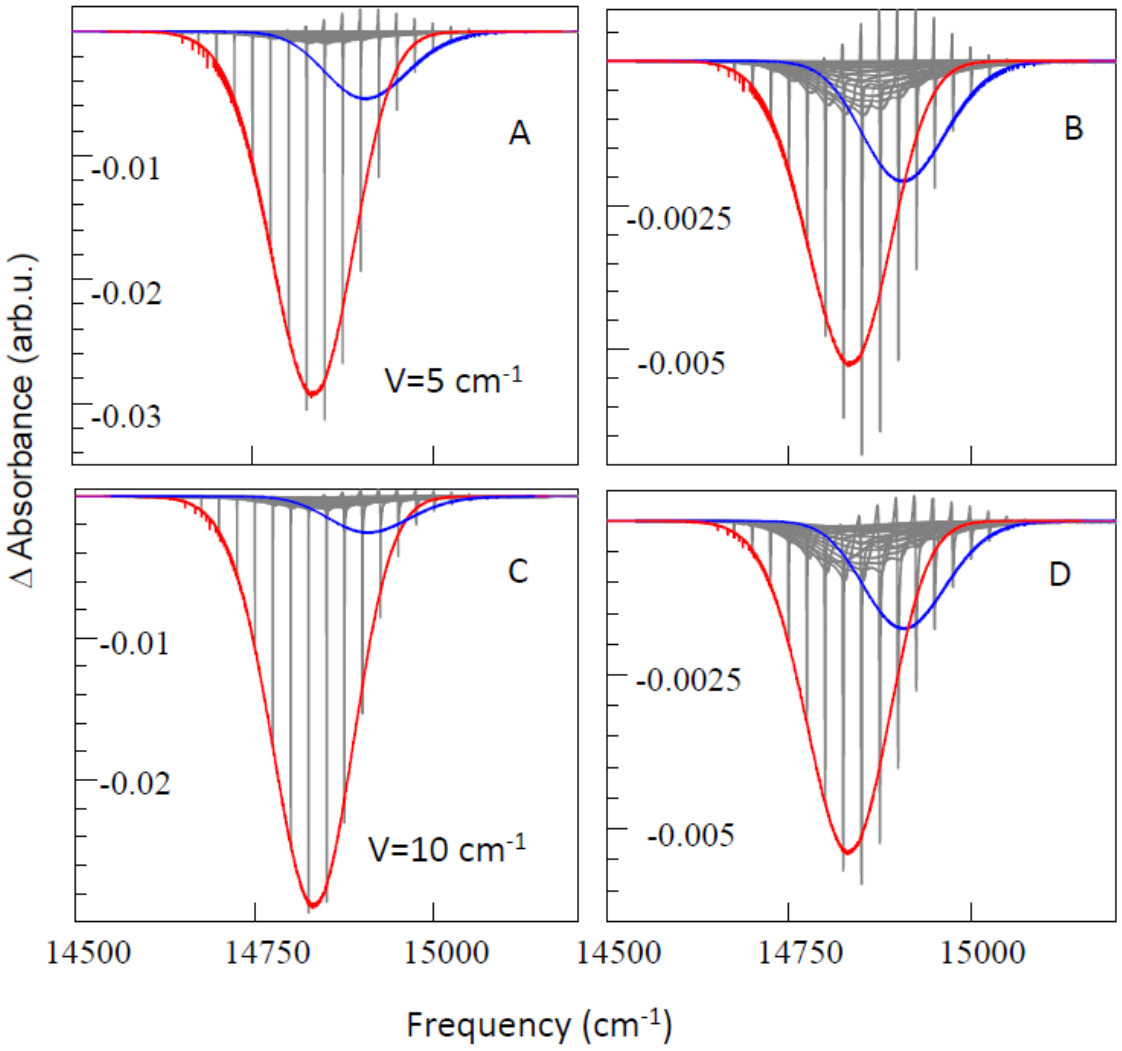

Figure 4. ZPH action spectra calculated for V=5 cm^{-1} (Frames A and B) and 10 cm^{-1} (Frames C and D) with resolution of 0.005 cm^{-1}(A and C) and 1 cm^{-1} (B and D). The SDF and electron-phonon coupling parameters were the same as in Figure 3. It was assumed that the burning mechanism involves formation of the Chl^{+} radical absorbing at about 830 nm.

3.4. Small Spectral Shifts Typically Observed for Resonant NPHB

The anti-hole functions for the "direct" burn employed so far feature large spectral shifts. Shifts of several tens to hundreds of cm^{-1} were observed in the case of the non-resonant NPHB in FMO[32], Photosystem I[33] and LH2[34] and in the single-molecule spectroscopy experiments on LH2[35]. Smaller shifts of about 10 cm^{-1} are dominant upon resonant NPHB. These differences are

likely due to the NPHB on more than one tier of the protein energy landscape[35,36]. For resonant burning, the NPHB on the smaller-shifts tier is more likely (since it is due to the tunneling through lower or narrower barriers), and it removes excited chromophores from the resonance with the laser, especially in the case of a blue spectral shift. In the case of non-resonant burning, the acceptor chromophore that has experienced a small spectral shift can still be excited non-resonantly, with very similar EET probability. Recently we published several papers demonstrating the presence of "spectral memory" in pigment-protein complexes such as Cyt b_6f and CP43 – spectral holes predominantly recover via burned chromophore-protein systems returning to the pre-burn configuration[29,36,37]. Thus, one may ask the following question – if the pigment that had experienced a small spectral shift remained the lower-E pigment and the "spectral memory" was indeed present– why wouldn't subsequent excitation via EET return the pigment-protein system back to its original configuration? Why wouldn't this effect cancel out both the NPHB of the lower-E state(s) following the EET and the associated additional burning into the higher excited states described in this work (indirect burn)? This is why: once the lower-E pigment's absorption shifts by any amount, the higher-E state shifts as well. Thus, if that higher-E state was in resonance with the narrow-band laser excitation to begin with, it will no longer be in resonance, and its probability to be excited again – to transfer energy downhill to its lower-E state partner and to cause its return to the pre-burn conformation – will be reduced.

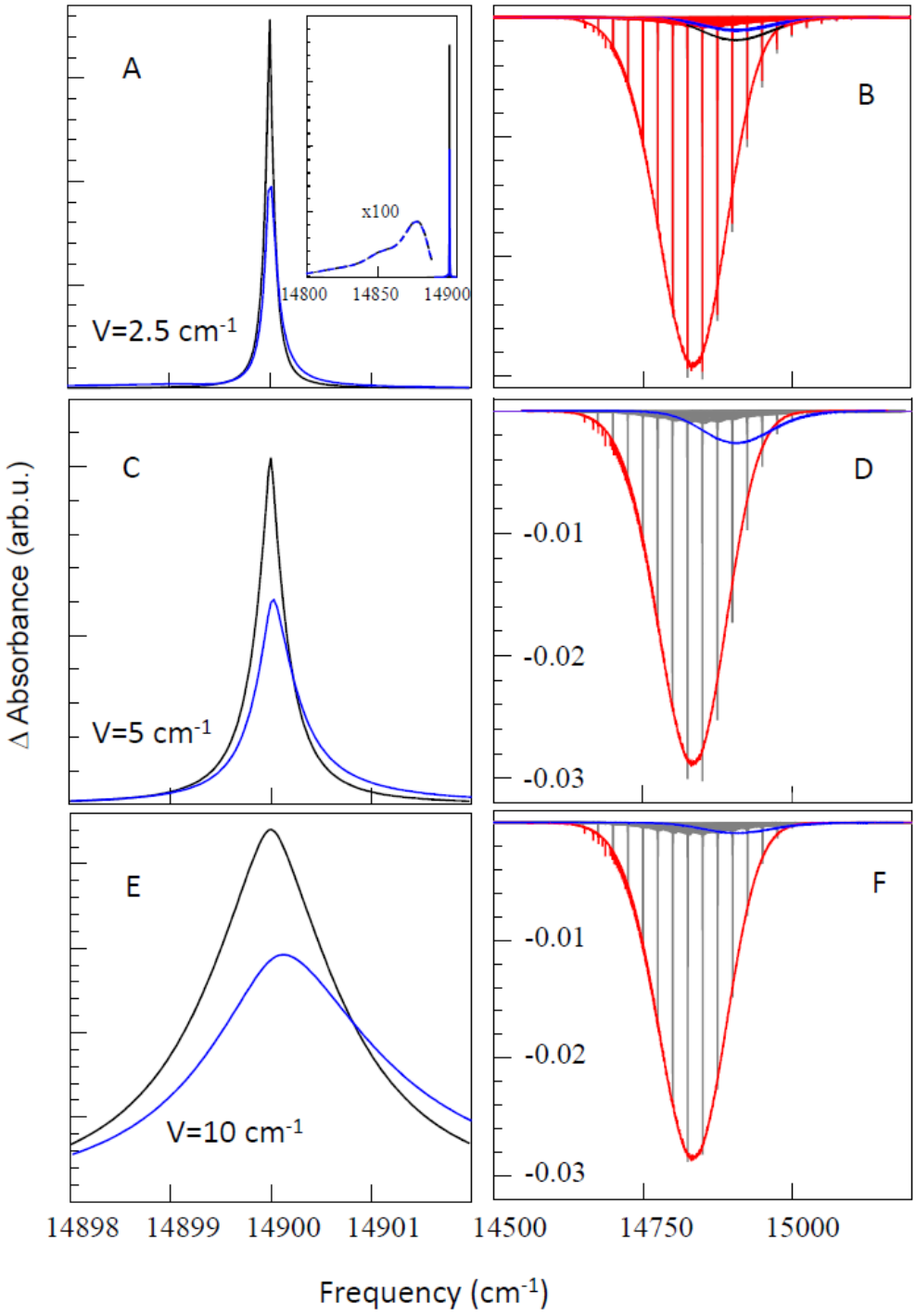

Figure 5. Distributions of excited donor molecules (black) for ω_B=14900 cm^{-1} and V=2.5 cm^{-1} (Frame A), 5 cm^{-1} (C) and 10 cm^{-1} (E). The insert in Frame A shows ZPL to PSB ratio. Blue curves are the results of convoluting the black curves with the anti-hole function for indirect burn. ZPH action spectra calculated for V=2.5 cm^{-1} (B) 5 cm^{-1} (D) and 10 cm^{-1} (F) with resolution of 0.005 cm^{-1}. Smooth solid red curve is the SDF of the acceptors. Black curve in Frame B represents the direct contribution of the donors to the ZPH action spectrum. Blue curve

represents the contribution from the indirect burn. The SDF and electron-phonon coupling parameters were the same as in Figure 3. The anti-hole function for "direct" burn was a Gaussian blue-shifted by 10 cm^{-1} and with the width of 30 cm^{-1}.

In Figure 5 we employed the direct-burn anti-hole function that is a Gaussian blue-shifted by just 10 cm^{-1} and with the FWHM of 30 cm^{-1}. Frames A, C and E show the distributions of the excited donors (black) clearly dominated by narrow ZPL-like features (see insert in Frame A). These were calculated for V = 2.5, 5 and 10 cm^{-1}, respectively. Also shown are the results of convoluting these distributions with the anti-hole functions for the indirect burn (such as those shown in Figure 2). These pre-burn (black) and post-burn (blue) excited donor distributions were normalized to the same area. Even a small shift of the lower-E pigment moves the higher-E state somewhat out of resonance with the excitation. Figure 5 also depicts the 0.005 cm^{-1}-resolution ZPH action spectra (Frames B, D, F) for V=2.5, 5 and 10 cm^{-1}, respectively. As can be seen, even on this protein energy landscape tier, the indirect burn effect is noticeable in some range of V.

4. Discussion

We start by clarifying the issue of the correlation between the ZPL frequencies of donors and acceptors. When excitation is in the donor-dominated frequency range, a subset of donors is excited selectively. The ZPL frequencies of donors and acceptors are uncorrelated, and consequently the NPHB of the acceptor molecules excited via EET results in a broad spectral hole. Similarly, direct resonant burning into the acceptor-dominated lower-frequency region results in a broad response from the higher-E states [24]. However, only the donors that were excited in the first place and whose acceptor partners were excited via EET and experienced NPHB participate in the "indirect burn", and these donors were frequency-selected.

As demonstrated above, the indirect burn effect enhancing the observable rate of burning into the donor bands is present for a wide variety of realistic anti-hole functions. In all cases, with decreasing *V*, one must eventually arrive to the situation where the higher-E state shifts become smaller than the dephasing-limited line width and the indirect burn effect disappears. On the other hand, for higher *V*, the magnitude of the difference in ZPH action spectra associated with the indirect burn effect is also decreasing with *V* (Figures 3-5). This is because the higher-E state spectral shifts increase proportionally to *V*, while the respective ZPL/ZPH widths increase proportionally to V^2. Thus, with the increase of *V*, a larger fraction of the higher excited states experience spectral shifts that are smaller than the EET-based hole width. For the same *V*, the difference between the NPHB action spectra (such as shown in Figures 3-5) should be larger for narrower SDF. The exact value of *V* for which the indirect burn effect will be largest is a result of a complex interplay between SDF width, $\Gamma_{dephasing}$, anti-hole function for the direct burn, and other model parameters. For parameters used to calculate the spectra in Figure 3 this optimal coupling appears to be around 2.5 cm^{-1}; for Figure 5 it is around 5 cm^{-1}. Employing more sophisticated EET theories may affect the calculated hole widths in a systematic manner and shift that optimal value of *V*. However, for low enough *V* the differences between EET rates calculated in Förster and modified Redfield approximations, for example, are small, except for the small subset of the dimers or trimers with very small initial differences in site energies[21,22]. Due to the site energy disorder most energy gaps are large enough and only a small fraction of the aggregates exhibit EET rates deviating from the Förster ones.

So far it was assumed that once the excitation reached the lowest-E pigment directly or via EET, the lowest-state NPHB was equally likely. This may not be true, as was pointed out by Adolphs et al.[20] They argued that the excess energy dissipated in the process of EET may help

the pigment-protein system sample a larger region of the energy landscape. This could provide not only a broad anti-hole function for the NPHB following the EET to the lowest-E state, but also more channels for NPHB and/or additional possibilities to cross the same barriers by activated process rather than tunneling[29,36,37]. Therefore, the NPHB yield for pigments excited via EET and the yield of the indirect burn effect may be even larger than the lowest-state resonant NPHB yield.

Note that when a significant fraction of the higher-E states experience spectral shifts smaller than the hole width, the shape of the spectral hole may be affected. Awareness of the indirect resonant burn effect is required if one wants to utilize the NPHB data (e.g. a series of holes burnt with an increasing dose or the dependence of hole width on the hole depth[12]) for determining the distribution of the EET rates. Suppose one uses the experimental data with a large contribution (due to the indirect burn) from the broad holes burnt into the donor states (see Figure 3B) and feeds that data into the model that does not take the indirect burn effect into account (e.g. [12]). The distribution necessary to obtain the match to the experimental data will be skewed towards shorter EET times and larger inter-pigment couplings. This will happen because one would have to believe that the observable broad holes are the narrowest donor holes there are, and that there is a whole higher-EET rate end of the distribution that burns even more poorly since its NPHB is supposed to be suppressed due to the EET rate term in the denominator of the NPHB yield (Eq. 1). While in fact this would be incorrect.

5. Conclusions

The NPHB of the lowest-E pigment in a coupled pigment system (following the EET from the higher-E states, which are excited directly) causes the shifts of the higher-E excited states. These

shifts contribute to the apparent rate of the resonant hole burning in donor-dominated regions at higher frequencies (thus affecting the ZPH action spectra) and modify the spectral hole widths and the EET times (or distributions thereof) derived by measuring the widths of the spectral holes.

Our hybrid approach includes both Monte-Carlo and NPHB master equation[9] features and allows for the inclusion of exciton effects (spectral shifts of all excited states of the system as a result of a shift of one site energy) into the calculations performed with very high spectral resolution (0.0048 cm^{-1} vs ~1 cm^{-1} in previous works) on a personal computer. This resolution is several times better than the 5 K homogeneous line widths observed for the lowest-E (free of further EET) states of the photosynthetic complexes. This software is capable of modeling the finest details of the experimental NPHB data. Other aspects of NPHB modeling (e.g. the two-tier distributions of the barriers on the protein energy landscape [36]) are fully integrated into the new software and could be turned on when calculations are performed on a more powerful computer. This would allow for exploring relative importance of various effects in NPHB and for quantitative modeling of real experimental data. Additional features of the excitonic calculations (e.g. redistribution of the oscillator strengths, the details of which depend on mutual orientation of the pigments in a particular pigment-protein complex) can also be implemented easily. The software is available to interested researchers upon request.

Acknowledgments:

Support from NSERC (under Discovery grant to VZ) is acknowledged. RJ acknowledges support from the Chemical Sciences, Geosciences and Biosciences Division, Office of Basic Energy Sciences, Office of Science, U.S. Department of Energy (Grant No. DE-SC0006678).

Supplementary Materials:

Details of the modeling procedure, effect of the λ-distribution on the ZPH action spectra and examples of the Δ-FLN spectra.

References:

1. Kharlamov, B. M.; Personov, R. I.; Bykovskaya, L. A.; Stable ‘Gap’ in Absorption Spectra of Solid Solutions of Organic Molecules by Laser Irradiation. *Opt. Commun.* **1974**, *12*, 191-193.
2. Gorokhovskii, A. A.; Kaarli, R. K.; Rebane, L. A.; Hole Burning in the Contour of a Pure Electronic Line in a Shpol'skii System. *JETP Lett.* **1974**, *20*, 216-217.
3. Szabo, A. Laser-Induced Fluorescence-Line Narrowing in Ruby**.** *Phys. Rev. Lett*. **1970**, *25*, 924-926.
4. Personov, R. I.; Al’shitz, E. I.; Bykovskaya, L. A.; The Effect of Fine Structure Appearance in Laser-excited Fluorescence Spectra of Organic Compounds in Solid Solutions. *Opt. Commun.***1972**, *6*, 169-173.
5. Yaaniso R. V.; Avarmaa, R. A. Measurement of the Inhomogeneous Distribution Function and Homogeneous Spectra of an Impurity Molecule in a Glassy Matrix. *J. Appl. Spectrosc*. **1986**, *44*, 365-370.
6. Fünfschilling, J.; Glatz, D.; Zschokke-Gränacher, I. Hole-burning Spectroscopy as a Tool to Eliminate Inhomogeneous Broadening. *J. Lumin.* **1986**, *36*, 85-92.
7. Reppert, M.; V. Naibo, V.; Jankowiak, R. Accurate Modeling of Fluorescence Line Narrowing Difference Spectra: Direct Measurement of the Single-Site Fluorescence Spectrum. *J. Chem. Phys.* **2010**, *133*, 014506.
8. Pieper, J.; Artene, P.; Rätsep, M.; Pajusalu, M.; Freiberg, A.; Evaluation of Electron-Phonon Coupling and Spectral Densities of Pigment-Protein Complexes by Line-Narrowed Optical Spectroscopy. *J. Phys. Chem. B*, **2018**, *122*, 9289–9301.
9. Jankowiak, R.; Reppert, M.; Zazubovich, V.; Pieper, J.; Reinot, T. Site Selective and Single Complex Laser-Based Spectroscopies: A Window on Excited State Electronic Structure,

Excitation Energy Transfer, and Electron-Phonon Coupling of Selected Photosynthetic Complexes. *Chem. Rev.* **2011**, *111*, 4546-4598.

10. Shu, L.; Small, G.J. Mechanism of Nonphotochemical Hole Burning: Cresyl Violet in Polyvinyl Alcohol Films. *J. Opt. Soc. Am.* B **1992**, *9*, 724-731.
11. Reinot, T.; Dang, N. C.; Small, G. J. A Model for Persistent Hole Burned Spectra and Hole Growth Kinetics that Includes Photoproduct Absorption: Application to Free Base Phthalocyanine in Hyperquenched Glassy Ortho-dichlorobenzene at 5 K. *J. Chem. Phys*. **2003**, *119*, 10404–10414.
12. Herascu, N.; Ahmouda, S.; Picorel, R.; Seibert, M.; Jankowiak, R.; Zazubovich, V. Effects of the Distributions of Energy or Charge Transfer Rates on Spectral Hole Burning in Pigment–Protein Complexes at Low Temperatures. *J. Phys. Chem.* B **2011**, *115*, 15098-15109.
13. Herascu, N., Kell, A., Acharya, K., Jankowiak, R., Blankenship, R. E., Zazubovich, V. Modeling of Various Optical Spectra in the Presence of Slow Excitation Energy Transfer in Dimers and Trimers with Weak Interpigment Coupling: FMO as an Example. *J. Phys. Chem.* B **2014**, *118*, 2032-2040.
14. Zazubovich, V.; Fluorescence Line Narrowing and Δ-FLN Spectra in the Presence of Excitation Energy Transfer between Weakly Coupled Chromophores. *J. Phys. Chem.* B **2014**, *118*, 13535−13543.
15. Tronrud, D. E.; Wen, J.; Gay, L.; Blankenship, R. E. The Structural Basis for the Difference in Absorbance Spectra for the FMO Antenna Protein from Various Green Sulfur Bacteria. *Photosynth Res.* **2009**, *100*, 79–87.
16. Yamashita, E.; Zhang, H.; Cramer, W.A. Structure of the Cytochrome b_6f Complex: Quinone Analogue Inhibitors as Ligands of Heme cn. *J. Mol. Biol.* **2007**, *370***,** 39-52.

17. Reppert, M.; V. Naibo, V.; Jankowiak, R. Modeling Study of Non-line-narrowed Hole-burned Spectra in Weakly Coupled Dimers and Multi-chromophoric Molecular Assemblies. *Chem. Phys.* **2010**, *367*, 27–35.
18. Reppert, M.; V. Naibo, V.; Jankowiak, R. Analytical Formulas for Low-fluence Non-line-narrowed Hole-burned Spectra in an Excitonically Coupled Dimer. *J. Chem. Phys.* **2009,** *131*, 234104.
19. Reppert, M. Modeling of Resonant Hole-Burning Spectra in Excitonically Coupled Systems: The Effects of Energy-Transfer Broadening. *J. Phys. Chem. Lett.* **2011**, *2*, 2716-2721.
20. Adolphs, J.; Berrer, M.; Renger, T. Hole-Burning Spectroscopy on Excitonically Coupled Pigments in Proteins: Theory Meets Experiment. *J. Am. Chem. Soc.* **2016**, *138*, 2993–3001.
21. Novoderezhkin, V.; van Grondelle, R., Spectra and Dynamics in the B800 Antenna: Comparing Hierarchical Equations, Redfield and Förster Theories. *J. Phys. Chem*. B **2013**, *117*, 11076−11090.
22. Yang, M.; Fleming, G. R., Influence of Phonons on Exciton Transfer Dynamics: Comparison of the Redfield, Förster, and Modified Redfield Equations. *Chem. Phys.* **2002**, *282*, 163–180.
23. Förster, T. Intermolecular Energy Migration and Fluorescence**.** *Ann. Phys.* **1984**, *2*, 55-75.
24. Kell, A.; Bednarczyk, D.; Acharya, K.; Chen, J.; Noy, D.; Jankowiak, R. New Insight into the Water-Soluble Chlorophyll-Binding Protein from *Lepidium virginicum*. *Photochem. Photobiol.* **2016**, *92*, 428–435.
25. Alster, J.; Lokstein, H., Dostál, J., Uchida, A.; Zigmantas, D. 2D Spectroscopy Study of Water-Soluble Chlorophyll-Binding Protein from *Lepidium virginicum. J. Phys. Chem.* B **2014**, *118*, 3524−3531.

26. Reinot, T.; Hayes, J. M.; Small, G. J. Laser-induced Hole Filling and Spectral Diffusion of Aluminum Phthalocyanine Tetrasulfonate in Hyperquenched Glassy Films. *J. Chem. Phys.* **1999**, *110*, 4820-4827.

27. Sener, M. K.; Lu, D.; Ritz, T.; Park, S.; Fromme, P.; Schulten, K. Robustness and Optimality of Light Harvesting in Cyanobacterial Photosystem I. *J. Phys. Chem. B* **2002**, *106*, 7948-7960.

28. Pullerits, T.; Hess, S.; Herek, J. L.; Sundström, V. Temperature Dependence of Excitation Transfer in LH2 of *Rhodobacter sphaeroides. J. Phys. Chem. B* **1997**, *101*, 10560-10567.

29. Najafi, M.; Herascu, N.; Shafiei, G.; Picorel, R.; Zazubovich, V. Conformational Changes in Pigment-Protein Complexes at Low Temperatures – Spectral Memory and a Possibility of Cooperative Effects. *J. Phys. Chem. B* **2015**, *119*, 6930−6940.

30. Kell, A.; Feng, X.; Reppert, M.; Jankowiak, R. On the Shape of the Phonon Spectral Density in Photosynthetic Complexes. *J. Phys. Chem.* B **2013**, *117*, 7317–7323.

31. Pieper, J.; Rätsep, M.; Trostmann, I.; Schmitt, F.-J.; Theiss, C.; Paulsen, H.; Eichler, H.J.; Freiberg, A.; Renger, G. Excitonic Energy Level Structure and Pigment-Protein Interactions in the Recombinant Water-Soluble Chlorophyll Protein. II. Spectral Hole-Burning Experiments. *J. Phys. Chem.* B **2011**, *115*, 4053–4065.

32. Johnson, S. G.; Small, G. J. Excited-State Structure and Energy-Transfer Dynamics of the Bacteriochlorophyll *a* Antenna Complex from *Prosthecochloris aestuarii*. *J. Phys. Chem*. **1991**, *95*, 471−479.

33. Zazubovich, V.; Matsuzaki, S.; Johnson, T. W.; Hayes, J. M.; Chitnis, P. R.; Small, G. J. Red Antenna States of Photosystem I from Cyanobacterium *Synechococcus elongatus*: a Spectral Hole Burning Study. *J. Chem. Phys*. **2002**, *275*, 47–59.

34. Grozdanov, D.; Herascu, N.; Reinot, T.; Jankowiak, R.; Zazubovich, V. Low-Temperature Protein Dynamics of the B800 Molecules in the LH2 Light-Harvesting Complex: Spectral Hole Burning Study and Comparison with Single Photosynthetic Complex Spectroscopy. *J. Phys. Chem.* B **2010**, *114*, 3426-3438.

35. Hofmann, C.; Aartsma, T. J.; Michel, H.; Köhler, J. Direct Observation of Tiers in the Energy Landscape of a Chromoprotein: A Single-molecule Study. *Proc. Natl. Acad. Sci. USA* **2003**, *100*, 15534-15538.

36. Levenberg, A.; Shafiei, G.; Lujan, M. A.; Giannacopoulos, S.; Picorel, R.; Zazubovich, V. Probing Energy Landscapes of Cytochrome b_6f with Spectral Hole Burning: Effects of Deuterated Solvent and Detergent. *J. Phys. Chem.* B **2017**, *121*, 9848-9858.

37. Najafi, M.; Herascu, N.; Seibert, M.; Picorel, R.; Jankowiak, R.; Zazubovich, V. Spectral Hole Burning, Recovery, and Thermocycling in Chlorophyll−Protein Complexes: Distributions of Barriers on the Protein Energy Landscape. *J. Phys. Chem.* B **2012**, *116*, 11780-11790.

TOC Graphic: